RSC Advances

ROYAL SOCIETY OF CHEMISTRY

www.rsc.org/advances

Atiya N. Jordan, Noureen Siraj, Susmita Das, Isiah M. Warner*

Tunable Near-Infrared Emission of Binary Nano- and Mesoscale GUMBOS

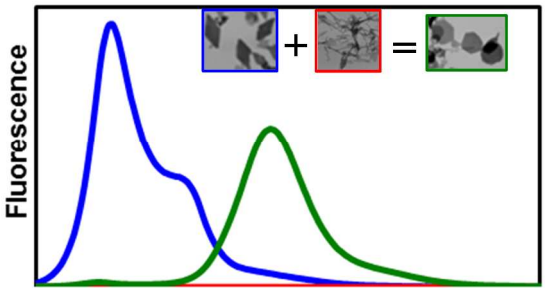

Mixtures of GUMBOS were used to form binary nanomaterials with tunable emission spectra due to Förster resonance energy transfer (FRET).

"Tunable Near-Infrared Emission of Binary Nano- and Mesoscale GUMBOS".

Atiya N. Jordan, Noureen Siraj, Susmita Das, Isiah M. Warner*

Department of Chemistry, Louisiana State University, Baton Rouge, LA 70803 (USA)

* Corresponding author: Isiah M. Warner,

email: iwarner@lsu.edu,

Phone: 1-225-578-2829

Abstract

Tuning the emission spectra of organic nanomaterials is of great interest due to possible use in sensing, optoelectronics, and light harvesting applications. Herein, we report tunable emission of binary organic nanomaterials derived from a **g**roup of **u**niform **m**aterials **b**ased on **o**rganic **s**alts (GUMBOS). In these studies, the cation of cyanine-based GUMBOS are altered by use of an increase in the alkyl groups of an attached methine chain. Mixtures of these GUMBOS are used to form binary nanomaterials, which are then characterized by use of UV-Vis absorption spectroscopy, fluorescence spectroscopy, and cyclic voltammetry. Based on these studies, it is determined that these binary nanomaterials exhibit broad absorption spectra, as well as tunable emission spectra due to the presence of Förster resonance energy transfer (FRET). This tunable emission of binary nanomaterials suggests potential applications as sensitizers in the visible to near-infrared region of the electromagnetic spectrum. Furthermore, examination of electrochemical properties indicates possible utility for light harvesting and optoelectronic applications.

Keywords: cyanine, aggregate, Förster resonance energy transfer, tunable fluorescence, light harvesting

Introduction

Nanomaterials, ranging from 1 to 100 nm, have gained considerable attention as compared to bulk materials due to higher surface area to volume ratios that result in distinct physiochemical properties. Research on such significant properties has led to innovative applications of engineered nanomaterials in areas such as medicine,[1-2] electronics,[3] and energy.[4-5] In particular, the use of organic nanomaterials to tune emission is of interest due to use in applications for sensing, optoelectronics, and light harvesting systems.

A common approach to tuning the emission spectra is based on Förster resonance energy transfer (FRET). This non-radiative process involves the transfer of energy from donor molecules in the excited state to acceptor molecules in the ground state.[6] The extent of FRET is dependent on the overlap of the donor emission spectrum and acceptor absorption spectrum, as well as the distance between the donor and acceptor. In this regard, Yao and coworkers have examined the use of organic nanomaterials to tune emission via FRET.[7-9] It was found that the energy transfer efficiencies of the nanomaterials were dependent on the molar ratios of the donor and acceptor molecules. These binary organic nanomaterials have demonstrated potential as candidates for applications in electroluminescent, optoelectronic, and sensing devices.

Our group has previously reported the formation of nanomaterials derived from a class of materials referred to as **g**roup of **u**niform **m**aterials **b**ased on **o**rganic **s**alts (GUMBOS).[10] These GUMBOS are solid phase organic salts composed of bulky, poorly coordinated ions that have melting points from 25°C to 250°C. The GUMBOS can be tailored for multiple functions based on the selected cations and anions. In addition, nanomaterials derived from GUMBOS (nanoGUMBOS) can also afford interesting physiochemical properties. Thus far, these

nanoGUMBOS have offered potential as candidates for biomedical,[10-13] antibacterial,[14] sensing,[15] optoelectronic,[16-17] and light harvesting[18-20] applications.

Several studies have been reported which involve the formation of nanoGUMBOS using cyanine dyes that form aggregates by self-assembly. Bwambok *et al.* initially observed that nanoGUMBOS containing heptamethine cyanine dye 1,1',3,3,3',3'-hexamethylindotricarbocyanine (HMT) iodide resulted in a broad absorption spectrum and slight shift in the fluorescence emission spectrum as compared to GUMBOS in solution.[11] These changes in the spectral properties were attributed to aggregation of the cationic near-infrared (NIR) dye. In addition, nanomaterials of the NIR fluorescent compound were employed as contrasting agents for biomedical imaging applications. In a subsequent study by Das *et al.*, variation of the anions paired with HMT was found to produce controlled aggregation and spectral properties.[18] The results further suggest the presence of aggregation, specifically of both J- and H- aggregates in different proportions. More recently, de Rooy *et al.* have reported the formation of nanostructures derived from thiacarbocyanine-based GUMBOS of increasing methine chain lengths.[19] Aggregation of these binary and ternary nanomaterials produced tunable fluorescence emission attributed to FRET.

Aggregation is the self-assembly of molecules as a result of forces such as van der Waals, hydrogen bonding, π-π stacking, and cation-π interactions. This self-assembly of molecules with such intermolecular interactions has been found to yield different types of aggregates leading to viable spectral properties. Such aggregation behavior has been well-studied by Davydov *et al.*[21] and Kasha *et al.*[22] Specifically, head-to-tail stacking of molecules results in the formation of J-aggregates that are generally characterized by a narrow, bathochromatically (red) shifted absorption band and enhanced fluorescence as compared to monomeric species. In contrast,

molecules stacked in a card-pack manner are referred to as H-aggregates. Such H-aggregates are typically characterized by a broad, hypsochromatically (blue) shifted absorption band with weak to no fluorescence. Molecules have also been found to form randomly-oriented aggregates without any specific order of stacking that exhibit spectral properties similar to the monomer.

In our previous work, pseudoisocyanine (PIC)-based nanoGUMBOS have been studied that exhibit controlled morphology and spectral properties at low concentration (30 μM) by simple variation of the counteranion.[20] This behavior was attributed to the presence of J- and H-aggregates. In the present work, PIC-based GUMBOS, the shortest methine chain length, and increased methine chain length cyanine-based GUMBOS were synthesized and investigated as binary nanomaterials. In these binary nanomaterials, previously studied PIC-based GUMBOS were selected as donor molecules due to enhanced emission within nanoGUMOBS, while increased methine chain cyanine-based GUMBOS were used as acceptor molecules. Interestingly, the higher methine chain cyanine-based nanoGUMBOS were essentially non-fluorescent in an aqueous environment. However, these materials were found to exhibit significant fluorescence as binary nanoGUMBOS which were attributed to the occurrence of FRET. The binary nanomaterials were found to have broad absorption and fluorescence emission extended to the near-infrared region by tuning the molar ratio. In addition, stability and electrochemical properties of these GUMBOS were also examined for potential use of these new materials for light harvesting and optoelectronic applications.

Materials and Methods

Materials

1,1’-diethyl-2,2’-cyanine iodide or pseudoisocyanine (PIC), 1,1’-diethyl-2,2’-carbocyanine iodide or pinacyanol (PC), 1,1’-diethyl-2,2’-dicarbocyanine (DD) iodide, and

lithium bis(trifluoromethanesulfonyl)imide ($LiNTf_2$) (99.95%) were purchased from Sigma Aldrich and used as received. Lithium bis(perfluoroethylsulfonyl)imide (LiBETI) was obtained from 3 M. Ethanol was purchased from Pharmaco-AAPER and used as received. Ultrapure water (18.2 MΩ cm) was used from Aries High Purity Water System. A BRANSON 3510RDTH model bath ulstrasonicator (335 W, 40 kHz frequency) was used at room temperature for syntheses of nanoGUMBOS. Carbon-coated copper grids (CF400-Cu, Electron Microscopy Sciences, Hatfield, PA) were used for TEM imaging.

Syntheses of Cyanine-based GUMBOS and NanoGUMBOS

Cyanine-based GUMBOS were synthesized by an anion exchange reaction of pseudoisocyanine (PIC) iodide, pinacyanol (PC) iodide, and 1,1'-diethyl-2,2'-dicarbocyanine (DD) iodide with $LiNTf_2$ and LiBETI using a method previously reported (Figure 1).[20] Binary nanomaterials were prepared for each anion by use of PIC GUMBOS as donors and increased methine chain GUMBOS (PC and DD) as acceptors. Different molar ratios of binary GUMBOS were prepared by keeping PIC donor GUMBOS constant while varying PC or DD GUMBOS. NanoGUMBOS were formed by use of a reprecipitation method in which 150 µL of the mixture of GUMBOS was added to 5 mL of DI water under sonication for 5 min. The nanomaterials were equilibrated for 10 min before analysis. This procedure was also used for synthesis of individual cyanine-based nanoGUMBOS.

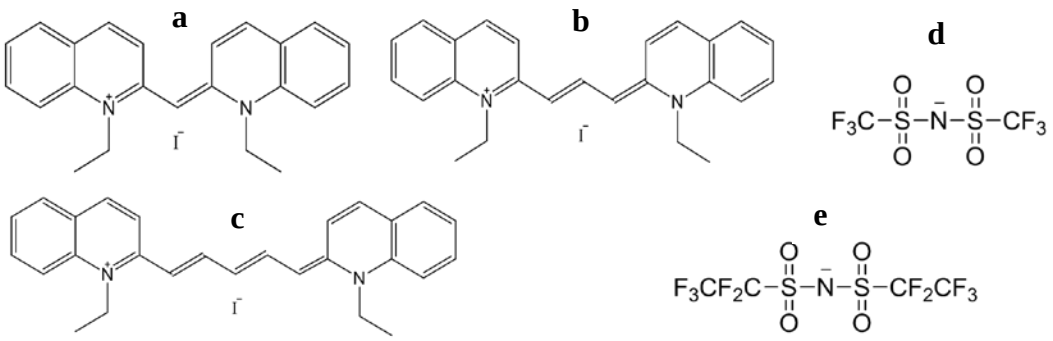

Figure 1. Chemical structures of parent compounds (a) PICI, (b) PCI, (c) DDI, and anions (d) NTf_2^- and (e) $BETI^-$.

Microscopy Characterization of NanoGUMBOS

Electron micrographs were obtained for characterization of size and morphology using a JEOL100CX transmission electron microscope (JEOL USA, Inc., Peabody, MA). An aliquot (5 µL) of nanoGUMBOS was dropcasted onto a carbon-coated copper grid and air dried at room temperature.

Absorption and Fluorescence Studies of GUMBOS and NanoGUMBOS

Absorbance measurements were obtained using a Shimadzu UV-3101PC UV-Vis-NIR scanning spectrometer (Shimadzu, Columbia, MD) at room temperature with a slitwidth of 2 nm. Fluorescence emission was performed on a Spex Fluorolog-3 spectrofluorometer (model FL3-22TAU3; Jobin Yvon, Edison, NJ) at room temperature with slitwidths of 5 nm. A 0.4 cm quartz cuvet (Starna Cells) was used to collect the absorbance and fluorescence measurements. A second 0.4 cm quartz cuvet was filled with water for use as a control blank. Fluorescence studies were all performed through adoption of a synchronous scan protocol with right angle geometry. Fluorescence spectra were corrected for inner filter effects using a standard formula.[6]

Stability Studies of GUMBOS and NanoGUMBOS

Photostability of individual and binary nanoGUMBOS was examined in aqueous suspension by use of fluorescence spectroscopy. Each sample was excited at an excitation

wavelength of 524 nm for 3000 s with wide slitwidths of 14 nm. Photostability of [PIC][BETI] and [PIC][NTf_2] nanoGUMBOS was based on specific emission wavelength maximum of 575 nm and 590 nm, respectively. Photostability of binary nanoGUMBOS was examined at an emission wavelength of 670 nm.

Thermal stability of the cyanine-based GUMBOS was investigated by use of thermograviometric analysis. Samples were measured under nitrogen at a rate of 10 °Cmin^{-1} with a temperature range from 23°C up to 600°C. Thermal decomposition of the cyanine-based GUMBOS started between 255°C and 325°C (Table 1). The onset temperatures (T_{onset}), at which samples lose weight at a faster speed, ranged from 353°C to 370°C. Overall, these results suggest that cyanine-based GUMBOS have good thermal stability.

Table 1. Thermal decomposition of cyanine-based GUMBOS

GUMBOS	T_{start} (°C)	T_{onset} (°C)
[PIC][NTf_2]	–	355
[PIC][BETI]	–	353
[PC][NTf_2]	325	370
[PC][BETI]	323	362
[DD][NTf_2]	248	363
[DD][BETI]	275	369

Electrochemical Studies of GUMBOS

Electrochemical measurements were performed under anaerobic conditions using an Autolab PGSTAT 302 potentiostat from Eco. Chemie. A three-electrode system consisting of an Ag/Ag^+ reference electrode, Pt working electrode, and Pt counter electrode was employed. Measurements were conducted in acetonitrile with 0.1 M tetrabutylammonium hexafluorophosphate ($TBAPF_6$) as a supporting electrolyte and ferrocene (Fc^+/Fc) as an internal reference having a formal potential of 0.63 V vs normal hydrogen electrode (NHE).

Results and Discussion

Morphological Studies of Cyanine NanoGUMBOS

Examination of TEM micrographs of cyanine-based nanoGUMBOS resulted in varying morphologies (Figure 2). The distinct diamond-like structure was found to exhibit an average respective length and width of 449 ± 96 nm and 241 ± 63 nm. The nanorods of [PIC][BETI] presented an average length and width of 1.6 ± 0.98 μm and 153 ± 55 nm, respectively. The dimensions of these nanoGUMBOS were similar to values previously reported, except for the width of [PIC][BETI]. This change in morphology was attributed to ordered molecular orientation as a function of the associated counteranion.[20] Nanomaterials of increased methine chain lengths afforded similar morphologies of nanowires and nanorods based on the selected anion. The [PC][NTf_2] and [DD][NTf_2] nanoGUMBOS formed nanowires with respective average lengths and widths of 402 ± 117 nm and 27 ± 7.3 nm for [PC][NTf_2] and 275 ± 67 nm and 24 ± 9.8 nm for [DD][NTf_2]. In contrast, [PC][BETI] nanoGUMBOS were found to have a continuous nanowire network with a width of 46 ± 8.1 nm. Moreover, [DD][BETI] nanoGUMBOS resulted in elongated nanorods with respective average lengths and widths of 11 ± 2.1 μm and 287 ± 120 nm.

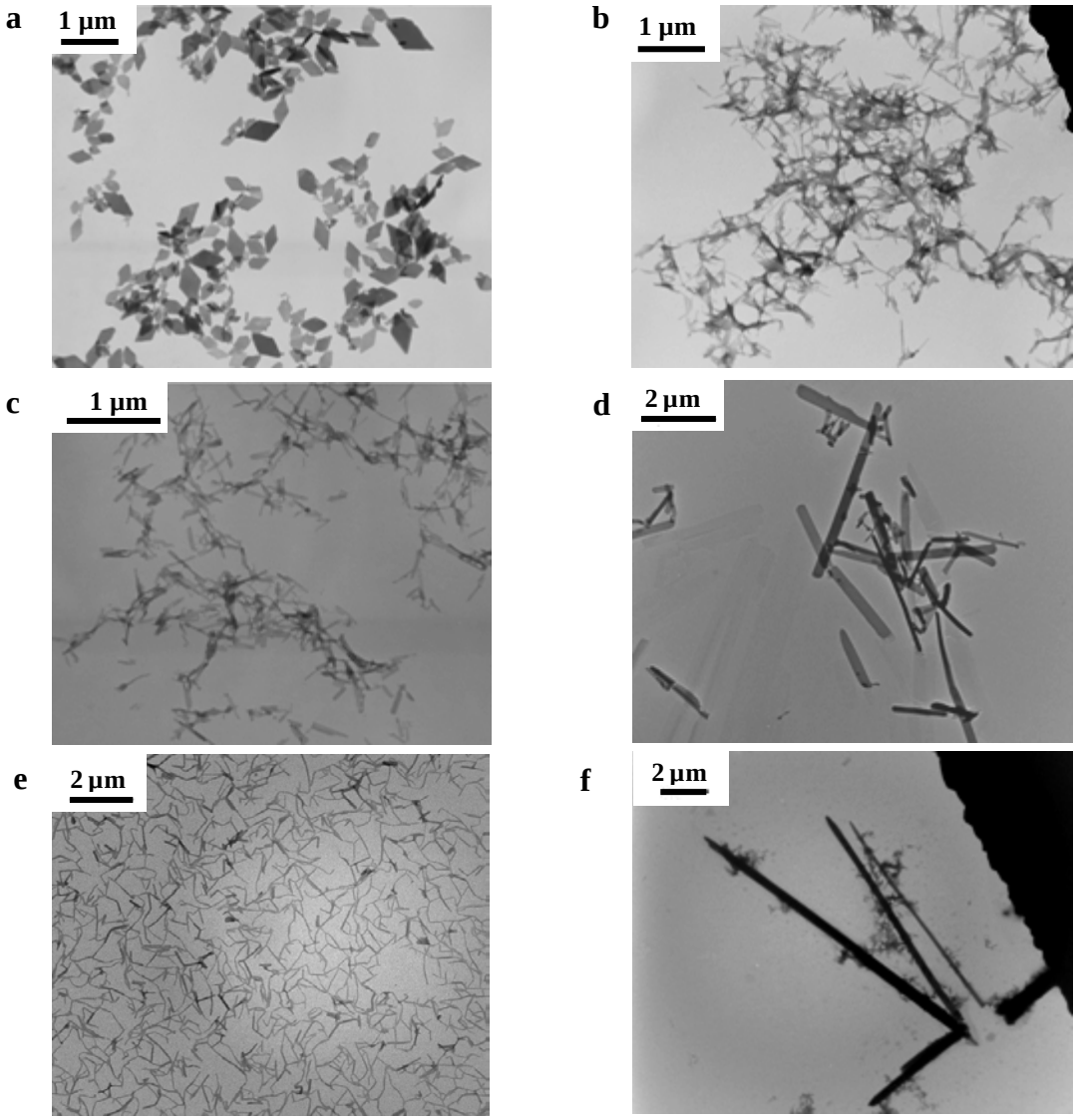

Figure 2. TEM micrographs of (a) [PIC][NTf_2], (b) [PC][NTf_2], (c) [DD][NTf_2], (d) [PIC][BETI], (e) [PC][BETI], and (f) [DD][BETI] nanoGUMBOS.

Spectral Properties of Cyanine NanoGUMBOS

Examination of absorption spectra of cyanine-based nanoGUMBOS resulted in a distinct change in aqueous dispersion as compared to cyanine-based GUMBOS in ethanolic solution. Absorption spectra of cyanine-based GUMBOS in ethanolic solution were found to exhibit red shifted absorption peaks as the methine chain length increased (Figure 3). Specifically, absorption peaks of 490 nm and 524 nm for PIC GUMBOS, 564 nm and 605 nm for PC

GUMBOS, as well as 652 nm and 710 nm for DD GUMBOS were obtained. It is important to note that this shift to longer wavelengths was independent of the associated anion. In contrast, absorption spectra of cyanine-based nanoGUMBOS resulted in broad absorption bands in aqueous dispersion that were dependent on both the methine chain length and associated anion (Figure 4). The [PIC][NTf_2] nanoGUMBOS were found to exhibit an absorption peak at 524 nm and a red shifted band at 590 nm, which is evidence of the formation of J-aggregates within the diamond-like nanostructures.[20] The absorption spectrum of [PC][NTf_2] nanoGUMBOS resulted in a blue shifted shoulder and peak at 490 and 550 nm, respectively. Conversely, longer wavelength and less intense absorption were observed for [DD][NTf_2] nanoGUMBOS with multiple peaks at 550, 650, and 695 nm. Interestingly, [PIC][BETI] and [PC][BETI] nanoGUMBOS were found to exhibit similar absorption spectra. The [PIC][BETI] nanoGUMBOS had absorption peaks at 490 and 524 nm, as well as a blue shifted peak at 450 nm with tail broadening in the longer wavelength region that were attributed to the formation of H-aggregates of the dye molecules within the nanorods.[20] The absorption spectrum of [PC][BETI] nanoGUMBOS resulted in peaks at 595 and 640 nm. In contrast, [DD][BETI] nanoGUMBOS displayed broad absorption with peaks at 515 and 605 nm. Overall, a blue shift in the absorption spectra was observed for the individual cyanine-based nanoGUMBOS as compared to cyanine-based GUMBOS in ethanolic solution. This result was attributed to the formation of H-aggregates within the nanomaterials and is in agreement with studies of PCCl and DDI in aqueous solution.[23-25]

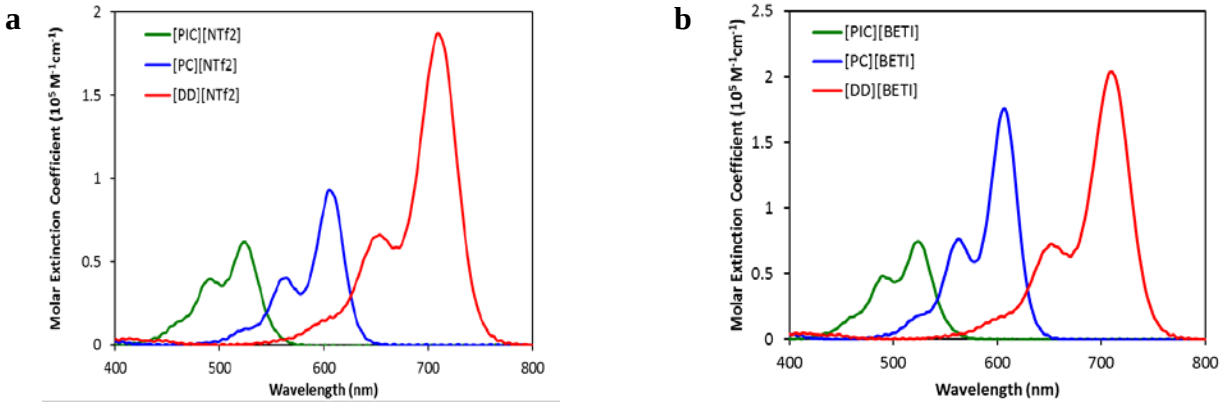

Figure 3. Absorption spectra of (a) NTf_2^- anion and (b) $BETI^-$ anion cyanine-based GUMBOS in ethanolic solution.

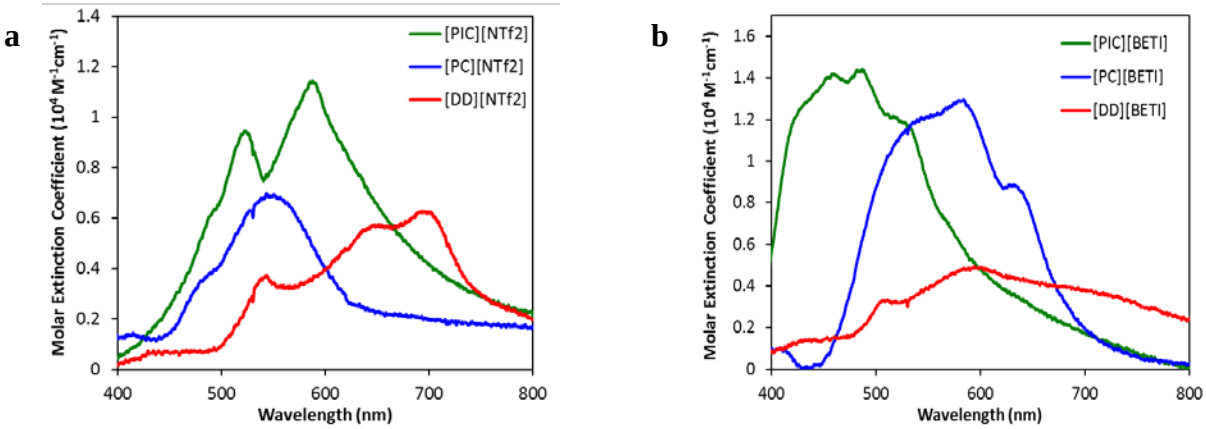

Figure 4. Absorption spectra of (a) NTf_2^- anion and (b) $BETI^-$ anion cyanine-based nanoGUMBOS in aqueous suspension.

Examination of fluorescence spectra was found to produce a distinct difference in the cyanine-based nanoGUMBOS with increasing methine chain length when excited at 524 nm (Figure 5). The [PIC][NTf_2] nanoGUMBOS resulted in a strong fluorescence peak at 590 nm, while nanoGUMBOS of [PIC][BETI] were found to exhibit a weaker fluorescence peak at ~577 nm. These PIC-based nanoGUMBOS of both anions also revealed a shoulder at 620 nm. This enhanced fluorescence of [PIC][NTf_2] nanoGUMBOS and weak fluorescence of [PIC][BETI] nanoGUMBOS, as compared to the parent compound of PICI in aqueous solution, were attributed to the formation of J- and H-aggregates, respectively.[20] In contrast, fluorescence spectra of increased methine chain length cyanine-based nanoGUMBOS resulted in minimal

fluorescence for both anions. The nanoGUMBOS of [PC][NTf_2], [DD][NTf_2], and [DD][BETI] were found to exhibit a nominal fluorescence peak at 630 nm. Furthermore, [PC][BETI] nanoGUMBOS were found to have a weak fluorescence at 702 nm. This little to no fluorescence confirms the formation of H-aggregates as observed in the absorption spectra.

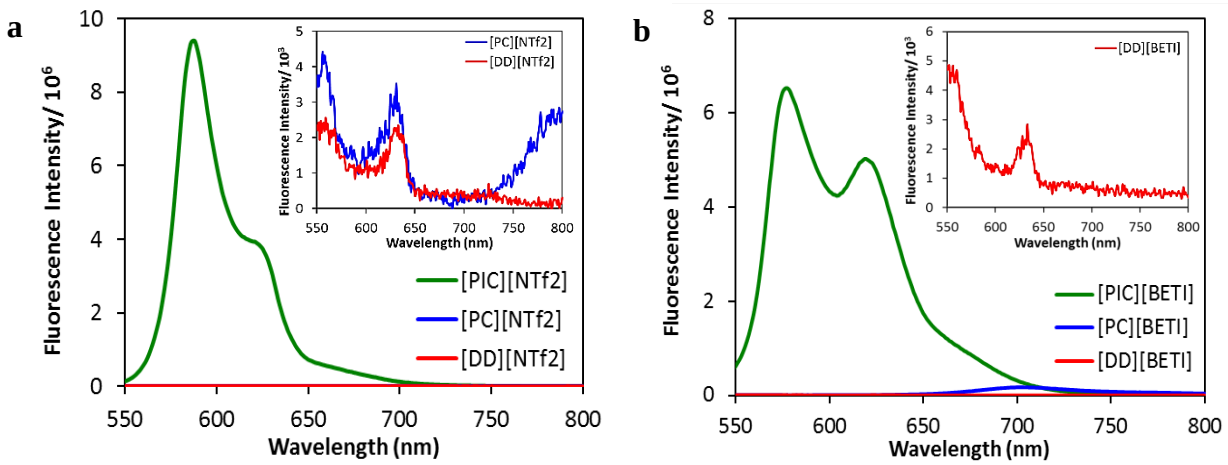

Figure 5. Fluorescence spectra of (a) NTf_2^- and (b) $BETI^-$ anion cyanine-based nanoGUMBOS in aqueous suspension when excited at 524 nm. Inset: Magnified fluorescence spectra of [PC][NTf_2] and [DD][NTf_2] shown in panel (a) and [DD][BETI] in panel (b).

Characterization Studies of Binary Cyanine NanoGUMBOS

Binary nanoGUMBOS were prepared from GUMBOS with similar anions by use of PIC GUMBOS as donor molecules and increased methine chain PC and DD GUMBOS as acceptor molecules. At an equal molar ratio, morphology of the binary nanomaterials resulted in different nanostructures based on the associated anions (Figure 6). Binary nanoGUMBOS containing NTf_2^- as an anion, namely [PIC][NTf_2]:[PC][NTf_2] and [PIC][NTf_2]:[DD][NTf_2], were found to have similar formation of hexagonal-shaped nanostructures with an average diameters of 161 ± 119 nm and 260 ± 44 nm, respectively. This was a distinct change in morphology as compared to the respective diamond-like nanostructures and nanowires of the individual cyanine-based nanoGUMBOS. In contrast, binary nanomaterials paired with $BETI^-$ anion afforded nanorod and nanowire structures. The [PIC][BETI]:[PC][BETI] nanoGUMBOS resulted in a network of

nanorods with a respective average length and width of 2.2 ± 0.75 μm and 115 ± 33 nm. The [PIC][BETI]:[DD][BETI] nanoGUMBOS were found to exhibit nanowires with a respective average length and width of 1.5 ± 0.85 μm and 101 ± 37 nm. These nanostructures also varied from the morphology of the nanorods and nanowires of the individual cyanine-based nanoGUMBOS.

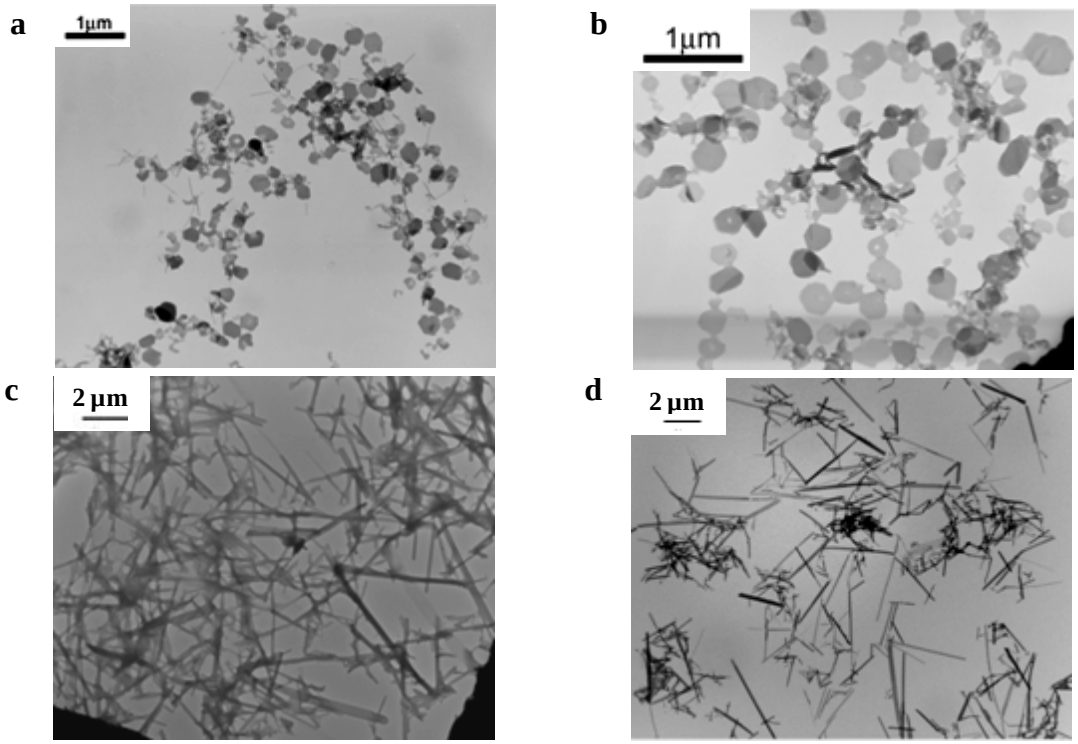

Figure 6. TEM micrographs of (a) [PIC][NTf_2]:[PC][NTf_2], (b) [PIC][NTf_2]:[DD][NTf_2], (c) [PIC][BETI]:[PC][BETI], and (d) [PIC][BETI]:[DD][BETI] binary nanomaterials at a 1:1 ratio.

Absorption Spectroscopy Studies

Absorption spectra of the binary nanomaterials at varying molar ratios were found to have similar spectral behavior as the donor absorption spectra of PIC nanoGUMBOS (Figure 7). Furthermore, additional absorption peaks were obtained for some of the binary nanoGUMBOS. In that regard, [PIC][NTf_2]:[PC][NTf_2] nanoGUMBOS resulted in a new absorption shoulder around 650 nm. Moreover, [PIC][BETI]:[PC][BETI] nanoGUMBOS were found to reveal absorption peaks for molar ratios of 1:1 and 10:1 at 595 and 640 nm resulting in further

broadening of the absorption spectra. This broadening was attributed to the acceptor absorption spectra of individual [PC][BETI] nanoGUMBOS.

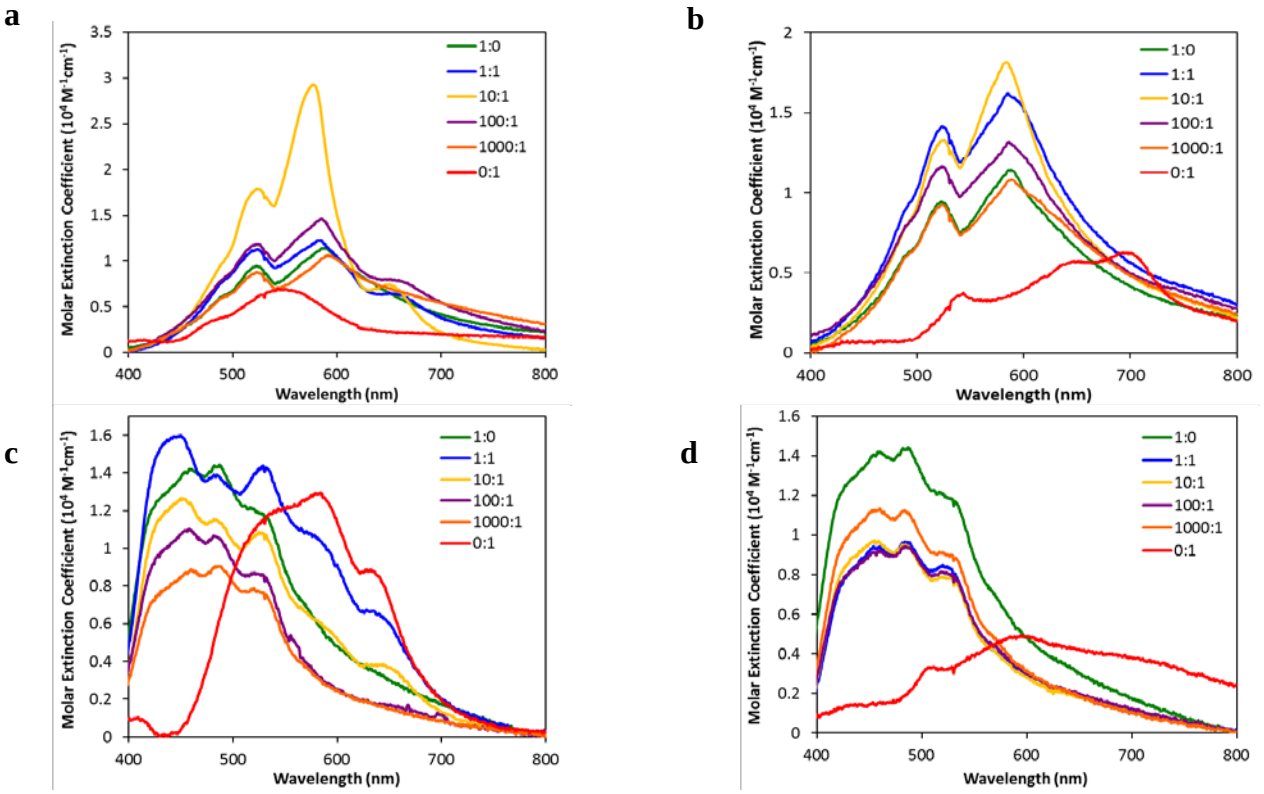

Figure 7. Absorption spectra of (a) [PIC][NTf_2]:[PC][NTf_2], (b) [PIC][NTf_2]:[DD][NTf_2], (c) [PIC][BETI]:[PC][BETI], and (d) [PIC][BETI]:[DD][BETI] binary nanoGUMBOS.

Fluorescence Spectroscopy Studies

The donor emission and acceptor absorption spectra of cyanine-based nanoGUMBOS suggested the possibility of FRET due to overlap of the absorption and fluorescence emission spectra (Figure 8). The spectral overlap integral (J(λ)) was determined using the following formula

$$J(\lambda) = \frac{\int_0^\infty \varepsilon(\lambda) f(\lambda) \lambda^4 d\lambda}{\int_0^\infty f(\lambda) d\lambda} \quad (1)$$

where ε is the molar extinction coefficient of the acceptor, f(λ) is the normalized emission spectrum of the donor, and λ is the wavelength. The energy transfer efficiency (E) was obtained using the following formula

$$E = 1 - \frac{F_{da}}{F_d} \quad (2)$$

where F_{da} and F_d are the fluorescence intensities of the donor in the presence and absence of the acceptor, respectively. The J(λ) and E values of the binary nanoGUMBOS at a 1:1 molar ratio are compiled in Table 2.

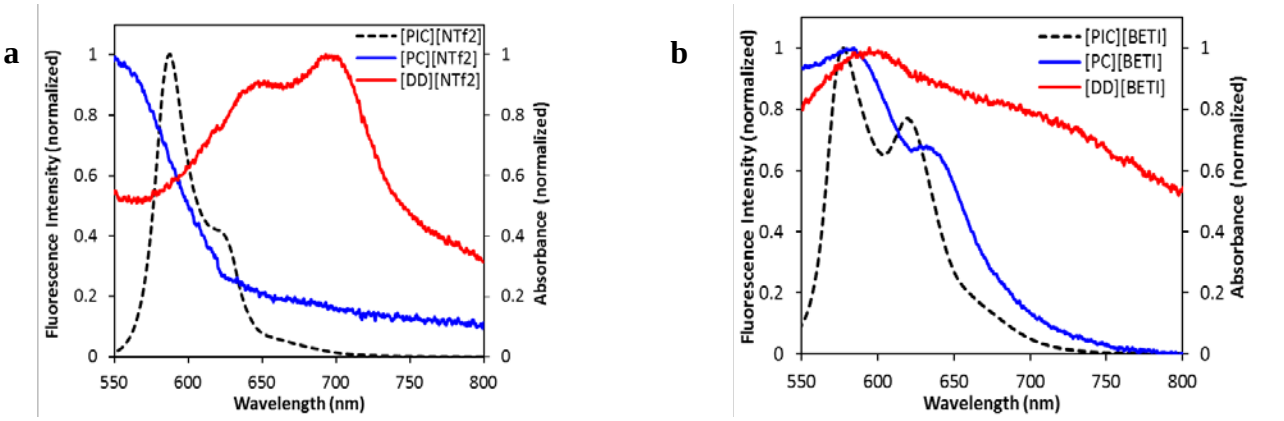

Figure 8. Normalized fluorescence (dashed) and absorption (solid) spectra of (a) NTf_2^- and (b) $BETI^-$ cyanine-based nanoGUMBOS in aqueous suspension.

Table 2. Spectral overlap integral (J(λ)) and energy transfer efficiency (E) of binary nanoGUMBOS at a 1:1 molar ratio

NanoGUMBOS	J(λ)/ $M^{-1}cm^{-1}nm^4$	% E
[PIC][NTf_2]: [PC][NTf_2]	3.86×10^{14}	99
[PIC][NTf_2]:[DD][NTf_2]	5.70×10^{14}	92
[PIC][BETI]: [PC][BETI]	1.30×10^{13}	99
[PIC][BETI]: [DD][BETI]	6.97×10^{14}	89

The highest spectral overlap integral value was obtained for [PIC][BETI]:[PC][BETI] nanoGUMBOS. Energy transfer efficiencies for binary nanoGUMBOS of both anions were found to exhibit high values of 99% in the case of PIC:PC nanoGUMBOS. These high energy transfer efficiencies were attributed to the compact environment of the nanomaterials, presence of J-aggregates from [PIC][NTf_2], and blue shifted absorption of the acceptor molecules due to the formation of H-aggregates. Binary nanomaterials containing the shortest and longest methine chains, [PIC][NTf_2]:[DD][NTf_2] and [PIC][BETI]:[DD][BETI], resulted in lower energy transfer efficiencies of 92% and 89%, respectively. These lower values of PIC:DD binary nanomaterials

were due to reduced spectral overlap as compared to PIC:PC binary nanoGUMBOS caused by broadening in the longer wavelength region.

Variations in the fluorescence spectra were observed for binary nanomaterials of both NTf_2^- and $BETI^-$ anions, which were formed with PIC as donor molecules in the presence of PC or DD as acceptor molecules. At an equal molar ratio, binary nanoGUMBOS were found to exhibit a new fluorescence peak at 670 nm, while resulting in a decrease of the donor fluorescence peak (Figure 9). The new emission peak was attributed to the occurrence of FRET from the PIC donor molecules to the acceptor molecules. This was a dramatic change from the little to no fluorescence of the individual nanoGUMBOS with longer methine chain lengths.

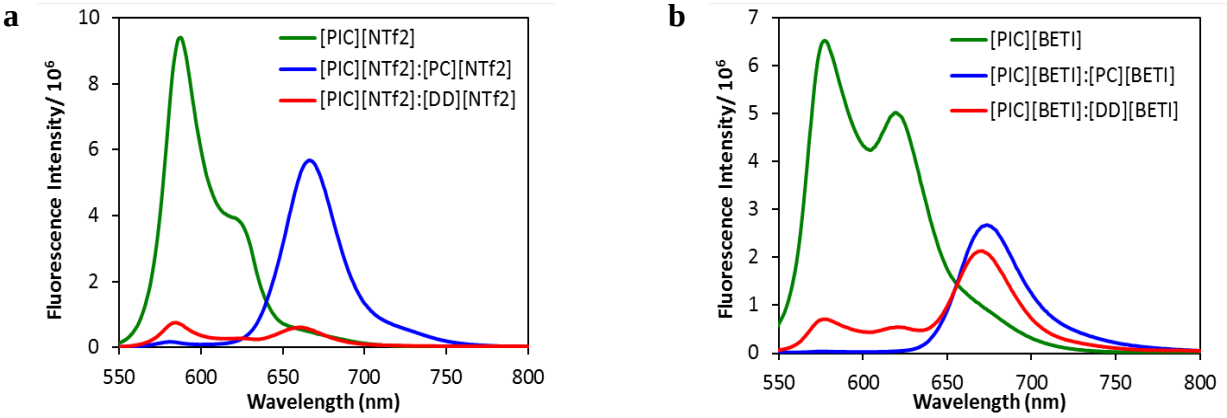

Figure 9. Fluorescence spectra of (a) NTf_2^- and (b) $BETI^-$ binary nanoGUMBOS in aqueous suspension at 1:1 molar ratio.

Binary nanoGUMBOS also resulted in tunable emission at different molar ratios with the same excitation wavelength of 524 nm (Figure 10). It was found that as the molar ratios of [PIC][NTf_2]:[PC][NTf_2] and [PIC][BETI]:[PC][BETI] binary nanoGUMBOS increased, the donor fluorescence peaks decreased while the acceptor fluorescence peaks increased due to FRET. In contrast, binary nanoGUMBOS containing DD as an acceptor initially resulted in a decrease in the donor fluorescence peaks and increase in acceptor fluorescence peak at a 1:1 molar ratio, followed by an increase in the donor peak and decrease in the acceptor peak at

higher molar ratios. This was due to a decrease in FRET since there was an abundance of donor molecules with respect to acceptor molecules. Interestingly, both donor and acceptor fluorescence peaks were observed for [PIC][NTf_2]:[PC][NTf_2] and [PIC][BETI]:[PC][BETI] binary nanoGUMBOS at a high molar ratio of 1000:1, which was also attributed to the abundance of donor molecules with respect to acceptor molecules. Furthermore, [PIC][NTf_2]:[DD][NTf_2] binary nanoGUMBOS at 1000:1 molar ratio were found to exhibit multiple fluorescence emission at different wavelengths, where a loss of fluorescence intensity at 670 nm resulted in a new fluorescence peak at 745 nm (Figure 10b). This spectral behavior revealed the ability to tune the emission wavelength of [PIC][NTf_2]:[DD][NTf_2] binary nanoGUMBOS to the near-infrared region. Thus, the extent of FRET in the various binary nanoGUMBOS demonstrated the wide range of tunability in emission wavelengths and intensities, which is suitable for numerous applications.

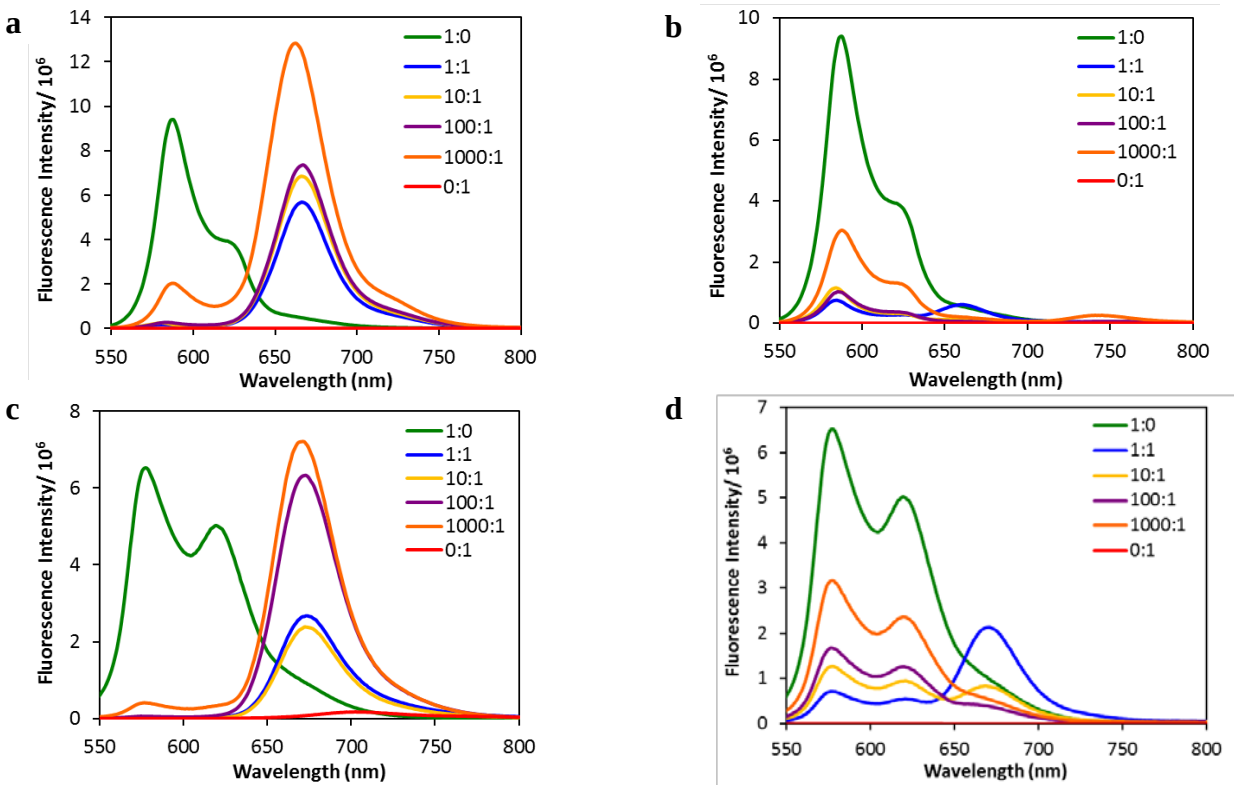

Figure 10. Fluorescence spectra of (a) [PIC][NTf_2]:[PC][NTf_2], (b) [PIC][NTf_2]:[DD][NTf_2], (c) [PIC][BETI]:[PC][BETI], and (d) [PIC][BETI]:[DD][BETI] binary nanoGUMBOS.

Photostability Analysis

Stability of dyes against degradation caused by light, heat, oxygen, and ozone is an important consideration for applications such as biomedical imaging, sensing, and light harvesting.[26] In that regard, photostability of PIC and binary nanoGUMBOS was studied and residual emission intensities were obtained (Figure 11). It is important to note that photostability of the individual increased methine chain cyanine-based nanoGUMBOS was not measured due to lack of fluorescence (Figure 5). The cyanine-based nanoGUMBOS were found to have residual emission intensities ranging from 53% to 113%. Specifically, gradual decrease was observed for [PIC][NTf_2] and [PIC][NTf_2]:[PC][NTf_2] nanoGUMBOS upon excitation for 3000 s with a residual emission intensity of 75% and 87%, respectively. Photostability of [PIC][NTf_2]:[DD][NTf_2] nanoGUMBOS increased in the first 120 s to 150% followed by a steady decrease with a residual emission intensity of 96%. In contrast, [PIC][BETI]

nanoGUMBOS resulted in a decrease in 240 s before reaching a plateau that resulted in a residual emission intensity of 53%. A residual emission intensity of 57% for [PIC][BETI]:[DD][BETI] nanoGUMBOS was obtained with a decrease in photostability in 720 s, followed by a slight increase before continuing to decrease. Conversely, photostability of [PIC][BETI]:[PC][BETI] nanoGUMBOS was found to exhibit the highest residual emission intensity of 113% due to gradual increase of the emission maximum over time. Generally, photostabilities of the cyanine-based nanoGUMBOS composed of NTf_2^- anions were higher than nanoGUMBOS of $BETI^-$ anions, with the exception for [PIC][BETI]:[PC][BETI] nanoGUMBOS. These higher photostabilities were attributed to the presence of J-aggregates from [PIC][NTf_2] and H-aggregates from [PIC][BETI], which is in agreement with studies of PEGylated cyanine-based nanoGUMBOS.[13]

Additionally, the binary nanoGUMBOS were found to be more photostable than the individual cyanine-based nanoGUMBOS with similar anions. This improved photostability was attributed to formation of a new excitation pathway via FRET. Variations in the initial emission intensity of the binary nanoGUMBOS were also observed. The increase in initial emission intensity of [PIC][NTf_2]:[DD][NTf_2] nanoGUMBOS was due to the presence of J-aggregate donor molecules and the occurrence of FRET (Figure 9). For [PIC][BETI]:[PC][BETI] nanoGUMBOS, the high photostability was attributed to greater spectral overlap and higher energy transfer efficiency as compared to nanoGUMBOS with a similar counteranion. In contrast, [PIC][BETI]:[DD][BETI] nanoGUMBOS were found to exhibit a decrease in initial emission intensity. This decrease corresponds to the presence of H-aggregate donor molecules as well as lower spectral overlap and energy transfer efficiency. Overall, the PIC and binary

nanoGUMBOS resulted in high photostability that suggest potential in light harvesting and optoelectronic applications.

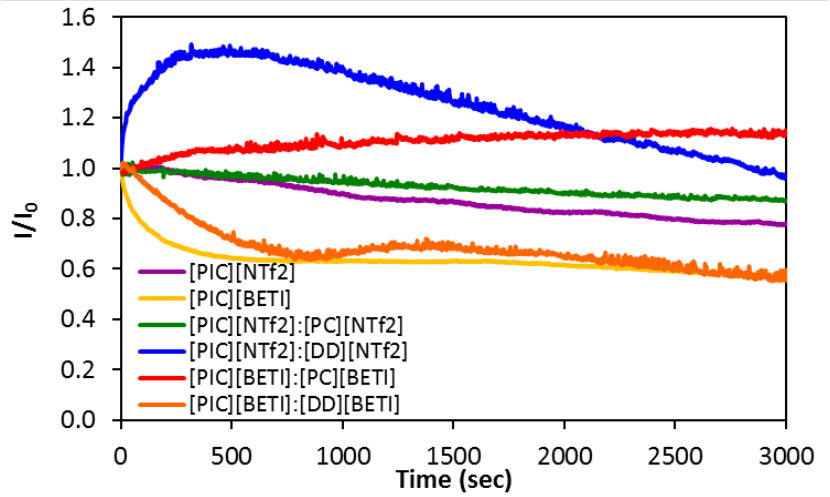

Figure 11. Photostability of cyanine-based nanoGUMBOS

Electrochemical Energy Levels and Band Gap Calculations

Cyclic voltammetry was performed for the cyanine-based GUMBOS in acetonitrile (Figure 12). Cyclic voltammograms of PIC GUMBOS revealed a reversible oxidation profile with a potential range from 1.1 V to 0.5 V. In contrast, a quasi-reversible oxidation profile was obtained for PC GUMBOS at potential ranges from 0.5 V to 0.1 V. A quasi-reversible oxidation profile was also displayed for DD GUMBOS with a potential range from 0.5 V to -0.2 V.

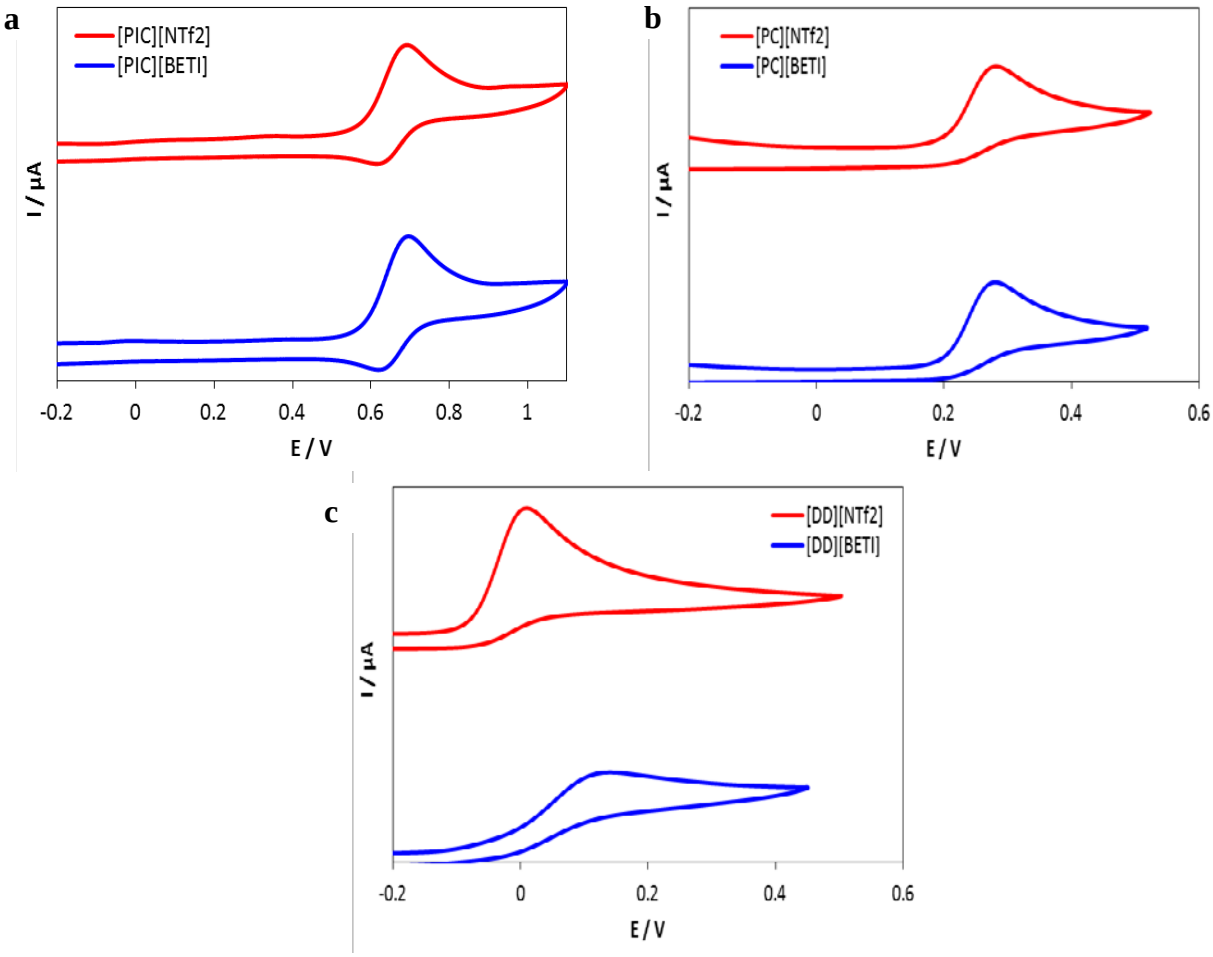

Figure 12. Cyclic voltammograms of (a) PIC, (b) PC, (c) DD GUMBOS (1 mM) in acetonitrile with 0.1 M $TBAPF_6$ vs Fc^+/Fc as a reference at 0.1 V/s.

Using the cyclic voltammograms, potentials and energy levels of the cyanine-based GUMBOS were obtained (Table 3). Due to the quasi-reversible profile, the oxidation potential (E_{ox}) was calculated from 85% of the maximum peak current. The excited state reduction potential (E^*_{red}) was determined using the oxidation potential by the following equations

$$E^*_{red} = E_{ox} - E_{0-0} \quad (3)$$

$$E_{0-0} = \frac{1240}{\lambda_{int}} \quad (4)$$

where $E_{0\text{-}0}$ represents the 0-0 transition energy state and λ_{int} is the intersect wavelength of the normalized absorption and emission spectra. Similar spectra were observed for both anions that revealed a red shift as the methine chain length increased. The λ_{int} of PIC, PC, and DD

GUMBOS was 539, 619, and 727 nm, respectively. The band gap of the cyanine-based GUMBOS was obtained by the onset wavelength (λ_{onset}) at which a negative tangent line of the lowest energy absorption peak intersects with a linear tangent line of the absorption tail. The λ_{onset} of PIC, PC, and DD GUMBOS was 556, 635, and 745 nm, respectively. Energy levels of the cyanine-based GUMBOS were calculated by the following equations

$$E_{HOMO}(eV) = -1e^{-}[E_{pa}(V\ vs\ Fc^{+}/Fc) + 4.8(V\ Fc^{+}/Fc\ vs\ Zero)] \quad (5)$$

$$E_{LUMO}(eV) = E_{HOMO} + E_g \quad (6)$$

where E_{HOMO} is the highest occupied molecular orbital (HOMO) energy level calculated versus vacuum with Fc^{+}/Fc as a reference and E_{pa} is the anodic potential. The lowest unoccupied molecular orbital energy level (E_{LUMO}) is obtained from the sum of the HOMO value and band gap.

The electrochemical properties of the cyanine-based GUMBOS revealed a decrease in oxidation potential with increased methine chain length. This resulted in a decrease in the HOMO energy level and reduced the band gap of the GUMBOS, which was expected due to the increase in wavelength as the methine chain length increased. The cyanine-based GUMBOS were found to have suitable potentials for possible application as sensitizers in dye-sensitized solar cells. The oxidation and excited state reduction potential of the dye are favorable for electron transfer to the conduction band of a titanium dioxide semiconductor (-0.5 V vs NHE), as well as an iodide/triiodide redox couple electrolyte (0.4 V vs NHE).

Table 3. Redox potentials and band gap of PIC GUMBOS obtained from UV-Vis absorption spectra

Dyes	E_{ox}[a] (V)	$E_{0\text{-}0}$[a] (V)	E^*_{red}[b] (V)	HOMO[c] (eV)	LUMO[c] (eV)	E_g (eV)
[PIC][NTf_2]	1.29	2.30	-1.01	-5.50	-3.27	2.23
[PIC][BETI]	1.31	2.30	-0.99	-5.56	-3.33	2.23
[PC][NTf_2]	0.962	2.00	-1.04	-5.13	-3.18	1.95
[PC][BETI]	0.972	2.00	-1.03	-5.14	-3.19	1.95
[DD][NTf_2]	0.632	1.71	-1.08	-4.80	-3.14	1.66
[DD][BETI]	0.701	1.71	-1.01	-4.87	-3.21	1.66

[a] The potentials were reported as V vs NHE. [b] The excited state reduction potential was obtained by equation $E^*_{red} = E_{ox} - E_{0-0}$. [c] The LUMO value was calculated by equation $E_{LUMO}(eV) = E_{HOMO} + E_g$.

Conclusion

In summary, variable methine chain length cyanine-based GUMBOS were synthesized to form binary nanomaterials with controlled morphology. These binary nanoGUMBOS were found to exhibit broad absorption and tunable emission for non-fluorescent acceptor molecules by changing the molar ratio due to the occurrence of FRET. Multiple fluorescence peaks were observed for [PIC][NTf_2]:[DD][NTf_2] nanoGUMBOS that extended to the near-infrared region. High energy transfer efficiencies were attributed to the compact environment of the nanomaterials, formation of J- and H-aggregates, and significant overlap of the absorption and emission spectra. Furthermore, high photostability and thermal stability were obtained for the binary materials. The tunable emission of these binary nanomaterials suggest interesting properties for potential applications in sensing and light harvesting in the visible to near-infrared region. In addition, electrochemical properties of the cyanine-based GUMBOS were observed to have suitable potentials for use as sensitizers in dye-sensitized solar cells. Moreover, the ability to tune these GUMBOS enables potential use in optoelectronics.

Acknowledgements

Atiya N. Jordan acknowledges support by a Board of Regents Fellowship from Louisiana State University. I.M.W. acknowledges the Philip W. West Endowment. This material is based upon

work supported by the National Science Foundation under grant no. (**CHE-0911118** and **DMR-0843962**). The authors thank Dr. Evgueni E. Nesterov for use of electrochemical instrumentation.

References

1. J. L. West; N. J. Halas, Annu. Rev. Biomed. Eng. 2003, 5, 285-292.
2. M. Goldberg; R. Langer; X. Q. Jia, J. Biomater. Sci.-Polym. Ed. 2007, 18 (3), 241-268.
3. Y. N. Xia; P. D. Yang; Y. G. Sun; Y. Y. Wu; B. Mayers; B. Gates; Y. D. Yin; F. Kim; Y. Q. Yan, Adv. Mater. 2003, 15 (5), 353-389.
4. A. S. Arico; P. Bruce; B. Scrosati; J. M.Tarascon; W. V. Schalkwijk, Nat. Mater. 2005, 4 (5), 366-377.
5. P. V. Kamat, J. Phys. Chem. C 2007, 111 (7), 2834-2860.
6. J. R. Lakowicz, Principles of Fluorescence Spectroscopy. 3 ed.; Springer: New York, 2006.
7. A. D. Peng; D. B. Xiao; Y. Ma; W. S. Yang; J. N. Yao, Adv. Mater. 2005, 17 (17), 2070-2073.
8. Y. S. Zhao; H. B. Fu; F. Q. Hu; A. D. Peng; W. S. Yang; J. N. Yao, Adv. Mater. 2008, 20 (1), 79-83.
9. J. Y. Zheng; C. A. Zhang; Y. S. Zhao; J. N. Yao, Phys. Chem. Chem. Phys. 2010, 12 (40), 12935-12938.
10. A. Tesfai; B. El-Zahab; A. T. Kelley; M. Li; J. C. Garno; G. A. Baker; I. M. Warner, ACS Nano 2009, 3 (10), 3244-3250.
11. D. K. Bwambok; B. El-Zahab; S. K. Challa; M. Li; L. Chandler; G. A. Baker; I. M. Warner, ACS Nano 2009, 3 (12), 3854-3860.
12. S. Das; S. L. de Rooy; A. N. Jordan; L. Chandler; I. I. Negulescu; B. El-Zahab; I. M. Warner, Langmuir 2012, 28 (1), 757-765.
13. C. Lu; S. Das; P. K. S. Magut; M. Li; B. El-Zahab; I. M. Warner, Langmuir 2012, 28 (40), 14415-14423.
14. M. R. Cole; M. Li; B. El-Zahab; M. E. Janes; D. Hayes; I. M. Warner, Chem. Bio. Drug Des. 2011, 78 (1), 33-41.
15. B. P. Regmi; J. Monk; B. El-Zahab; S. Das; F. R. Hung; D. J. Hayes; I. M. Warner, J. Mater. Chem. 2012, 22 (27), 13732-13741.
16. J. C. Dumke; B. El-Zahab; S. Challa; S. Das; L. Chandler; M. Tolocka; D. J. Hayes; I. M. Warner, Langmuir 2010, 26 (19), 15599-15603.
17. S. L. de Rooy; B. El-Zahab; M. Li; S. Das; E. Broering; L. Chandler; I. M. Warner, Chem. Commun. 2011, 47 (31), 8916-8918.
18. S. Das; D. Bwambok; B. Ei-Zahab; J. Monk; S. L. de Rooy; S. Challa; M. Li; F. R. Hung; G. A. Baker; I. M. Warner, Langmuir 2010, 26 (15), 12867-12876.
19. S. L. de Rooy; S. Das; M. Li; B. El-Zahab; A. Jordan; R. Lodes; A. Weber; L. Chandler; G. A. Baker; I. M. Warner, J. Phys. Chem. C 2012, 116 (14), 8251-8260.
20. A. N. Jordan; S. Das; N. Siraj; S. L. de Rooy; M. Li; B. El-Zahab; L. Chandler; G. A. Baker; I. M. Warner, Nanoscale 2012, 4 (16), 5031-5038.
21. A. S. Davydov, Theory of Molecular Excitons. McGraw-Hill: New York, 1962.
22. M. Kasha; H. R. Rawls; M. Ashraf El-Bayoumi, Pure Appl Chem 1965, 11, 371-392.

23. S. Y. Chen; M. L. Horng; E. L. Quitevis, J. Phys. Chem. 1989, 93 (9), 3683-3688.
24. S. Gadde; E. K. Batchelor; A. E. Kaifer, Chem. Eur. J. 2009, 15 (24), 6025-6031.
25. S. Barazzouk; H. Lee; S. Hotchandani; P. V. Kamat, J. Phys. Chem. B 2000, 104 (15), 3616-3623.
26. A. Mishra; R. K. Behera; P. K. Behera; B. K. Mishra; G. B. Behera, Chem. Rev. 2000, 100 (6), 1973-2011.